Cement and Concrete Composites 131 (2022) 104608

Contents lists available at ScienceDirect

Cement and Concrete Composites

journal homepage: www.elsevier.com/locate/cemconcomp

Durability of eco-efficient binary cement mortars based on ichu ash: Effect on carbonation and chloride resistance

Laura Caneda-Martínez [a,b,*], Moisés Frías [a,1], Javier Sánchez [a], Nuria Rebolledo [a], Elena Flores [c], César Medina [d,1]

[a] Eduardo Torroja Institute (IETcc-CSIC), C/ Serrano Galvache 4, 28033 Madrid, Spain
[b] Universidade da Coruña, Department of Civil Engineering, Campus de Elviña s/n, 15071 A Coruña, Spain
[c] Universidad de Ingeniería y Tecnología (UTEC), Jr Medrano Silva, Lima 04, Peru
[d] Universidad de Extremadura, Departamento de Construcción, Instituto de Investigación en Desarrollo Territorial Sostenible (INTERRA), Grupo de Investigación MATERIA, Avda. de la Universidad, s/n, 10003, Cáceres, Spain

ARTICLE INFO

Keywords:
Ichu ash
Biomass-based pozzolan
Blended cements
Durability
Chloride resistance
Carbonation

ABSTRACT

This research work focuses on the performance of mortars containing ichu ash as a potential environmentally-sound alternative to traditional pozzolans (at 6% and 10% replacement levels) under CO_2 and chloride ion rich environments, in order to evaluate the capacity of this material to produce more sustainable and durable blended cements. The results indicate that ichu ash increases the susceptibility to carbonation, although mortars with 6% ichu ash content behave similarly to OPC ones. However, both density and mechanical strength improve after 250 days of carbonation for both ichu-blended mortars. In terms of resistance to chloride penetration, the addition of ichu ash contributes to retaining the ions in the superficial layers of the mortars, inhibiting their advance. It was found that formulations with both 6% and 10% ichu ash content produced a reduction in the chloride diffusion coefficient of approximately 60%. This phenomenon was mainly attributed to the refinement and increased complexity of the microstructure of the mortars due to the pozzolanic effect. Therefore, it was found that in certain types of environments, ichu ash can be an interesting tool to improve the durability of cements while reducing their environmental footprint and exploiting local resources.

1. Introduction

The cement manufacturing process is known for its massive consumption of raw materials and energy, as well as for the vast amounts of CO_2 emissions associated with the activity [1,2]. This situation, coupled with the imperative need to take greater steps towards environmental protection, is resulting in increasing societal and political pressure to improve the sustainability of the cement industry. As a matter of fact, the cement sector has been developing tools to address this problem for decades, among which the use of supplementary cementitious materials (SCMs) has occupied a prominent role [3–5]. Nevertheless, the ever-growing demand for cement and the declining availability of traditional SCMs have triggered researchers to explore alternatives to reduce the cement-associated environmental footprint.

The use of vegetable ashes as SCMs is attracting interest as an option to contribute to turning the cement sector into a greener industry [6–9]. Their broad availability, low cost and excellent reactivity are some of the reasons behind their growing popularity [9]. Moreover, the advantages of this type of action transcend the cement industry, as they would also provide an environmentally sound route for the management of agro-industrial waste, preventing its unregulated burning and the problems associated with its uncontrolled accumulation in landfills (such as deterioration of land, air and water quality) [8,10,11]. In addition, certain vegetal resources are of particular value as raw material for energy generation in biomass-fired power plants [12,13]. This type of renewable and carbon-neutral energy source is emerging as a promising measure to address the impending energy crisis caused by the rising energy demand and the need for alternative and cleaner power generation methods. However, this type of activity faces major challenges in terms of managing the voluminous and abundant ashes generated as waste [14,15]. The exploitation of said ashes as pozzolans for cement entails the creation of a highly advantageous synergy

* Corresponding author. Universidade da Coruña, Department of Civil Engineering, Campus de Elviña s/n, 15071 A Coruña, Spain.
E-mail address: laura.cmartinez@udc.es (L. Caneda-Martínez).
[1] SOSMAT, Universidad de Extremadura, Partnering Unit to CSIC, Badajoz, España.

https://doi.org/10.1016/j.cemconcomp.2022.104608
Received 20 November 2021; Received in revised form 8 May 2022; Accepted 26 May 2022
Available online 29 May 2022

between these activities, stimulating the exploitation of biomass as an energy source and enhancing at the same time the sustainability of the cement sector. A noteworthy example of this type of cooperation was proposed for elephant grass, a plant of high calorific value and availability that has become an important source of energy production in Brazil, and whose ashes present excellent properties as supplementary cementitious material [16–19]. Sugarcane bagasse, a vegetable waste obtained in large quantities in the sugar and alcohol industry, is another interesting example, as its combustion provides a valuable source of energy and produces ashes with promising pozzolanic properties [20–26].

The pozzolanic reactivity of vegetable ashes has its origin in the silicon absorbed by plants during their lifetime from the soil or the groundwater, which is finally preserved in their ashes after combustion as amorphous silica [9,27]. Although all plants rooted in soil have the capacity to uptake silicon, this ability differs greatly depending on their species. Generally, the highest concentrations are found in monocotyledonous plants. Particularly, those of the order Poales and the family Poaceae (comprising vegetables such as grasses, cereals or bamboo) produce remarkable silicon accumulations [28,29]. Thus, vegetable ashes like those from rice husk, bamboo, wheat or the aforementioned elephant grass or sugarcane bagasse are the ones that have captured the attention of the cement industry [6–8,30,31].

Ichu grass is a monocot plant, of the order Poales and the family Poaceae, composed mainly of lignin, cellulose and hemicellulose [32,33]. It grows abundantly, without requiring cultivation, in the high Andean region. Even though it was once widely exploited by the local population as fodder for livestock or as raw material for the production of bricks, roofs or ropes, nowadays it has fallen into disuse [34]. Hence, ichu grass accumulates uncontrolled, even causing severe problems such as wildfires due to its high flammability. To reduce these risks and to benefit from this resource, alternative uses are being explored. Some proposed applications include the use of the grass as fibres for the production of biocomposites or of its ashes as SCM [32,34–36]. The latter case would involve calcination of the grass, which would be all the more interesting as the high volumes of ichu grown naturally, with low production costs, make it a good candidate for its exploitation for energy production.

Frias et al. [36] proved that the calcination of ichu grass yields silica-rich ashes of high pozzolanic activity. Its use as supplementary cementitious material at 6% and 10% substitution levels produced blended cements that comply with the physical requirements established in the current standards [37], although they also exhibited reduced mechanical properties. However, it was also found that ichu ash caused a significant increase in the complexity of the microstructure, which resulted in a reduction of pore connectivity and capillary sorption. These aspects are of great relevance as they provide indirect evidence of an increased ability to resist the introduction of harmful agents into the material and, thus, of improved durability.

The design of more durable materials is also a key step toward achieving sustainable economic models. Given that the use of ichu ash might contribute to improving the environmental footprint of cement, not only during its production but also throughout its service life, its effect on durable properties needs to be further explored. Consequently, this work focuses on the study of the behaviour of mortars made with blended cements containing 6% and 10% ichu ash under the action of two of the most relevant damaging agents to cement-based structures: CO_2 and chloride ions.

2. Materials and methods

2.1. Materials

The ichu grass used in this work was harvested in the Sicuani District, situated in the Department of Cuzco, Peru. After being collected, the leaves were selected and cleaned, then cut into approximately 1-cm portions and dried at 100 °C for 3 h. Lastly, they were thermally treated at 600 °C for 2 h to produce the ashes, as these were considered to be the appropriate calcination conditions for this type of material in previous studies [7,36].

The chemical composition of ichu ash is listed in Table 1. The ash is predominantly composed of SiO_2 (77.7%), although substantial amounts of K_2O (8.1%), CaO (3.70%) and P_2O_3 (2.9%) are also found. Other minority elements such as manganese, strontium, zinc, copper and chlorine are present at concentrations lower than 0.5%. As described in a previous work [36], the composition of ichu ash is dominated by amorphous silica, although crystalline compounds can be identified in its composition, mainly in the form quartz, calcite and sylvite. As reported in said work, ichu ash displays a good pozzolanic activity, which resembles that exhibited by silica fume. Regarding particle size distribution, ichu ash is defined by D_{10}, D_{50} and D_{90} values of 2.95, 13.3 and 39.2 μm, respectively, as shown in Fig. 1.

An ordinary Portland cement (OPC) type CEM I 42.5 R was used for this study, which was supplied by Cementos Portland Valderribas group, from its factory in El Alto (Madrid). Its chemical composition is described in Table 1, while its particle size distribution is given in Fig. 1 (D_{10} = 1.93, D_{50} = 18.5 and D_{90} = 69.2). Two blended cements were prepared by partial substitution of OPC for ichu ash in proportions of 6% (ICHU6) and 10% (ICHU10) by weight.

The mortars used in this work were prepared at a water/binder ratio of 0.5 and a sand/cement ratio of 3:1, following the guidelines established by EN 196-1 standard [38]. The standardised sand was defined by a minimum SiO_2 content of 98% and a maximum particle size of 2 mm.

2.2. Methods

2.2.1. Evaluation of chloride penetration resistance

Resistance to chloride ion penetration was assessed according to the procedure laid down in EN 12390-11 [39]. Accordingly, two cylindrical mortar specimens (7.5 × 15 cm) were prepared for each type of cement, and then cured in a humidity chamber for 90 days. Each specimen was divided into two sub-specimens (7.5 × 7.5 cm), which were each provided with a pond sealed with silicone on one of their circular faces. The ponds were filled with distilled water and maintained for 24 h, ensuring water-tightness. Subsequently, the pond was filled with a 30 g/L NaCl solution and kept sealed with a plastic film for another 90 days.

After the exposure period, powder samples were extracted at different depths in three of the four sub-specimens by profile grinding. Eight layers were extracted per specimen, at the depths recommended by the aforementioned standard for each type of cement. The samples were dried and then their acid-soluble chloride content was determined as described in EN 14629 [40], using a Mehtrom 888 Titrando

Table 1
Chemical composition of the starting materials.

Oxides (%)	Ichu ash	OPC
SiO_2	77.70	19.40
Al_2O_3	0.98	6.10
CaO	3.70	62.20
MgO	0.98	1.10
Fe_2O_3	0.49	2.40
SO_3	1.90	4.30
Na_2O	0.20	0.13
K_2O	8.10	1.10
TiO_2	0.09	0.24
P_2O_5	2.90	0.10
MnO	0.24	0.03
SrO	0.03	0.06
ZnO	0.02	0.04
CuO	0.01	0.02
Cl	0.42	0.02
LoI[a]	2.11	2.80

[a] LoI: Loss on ignition.

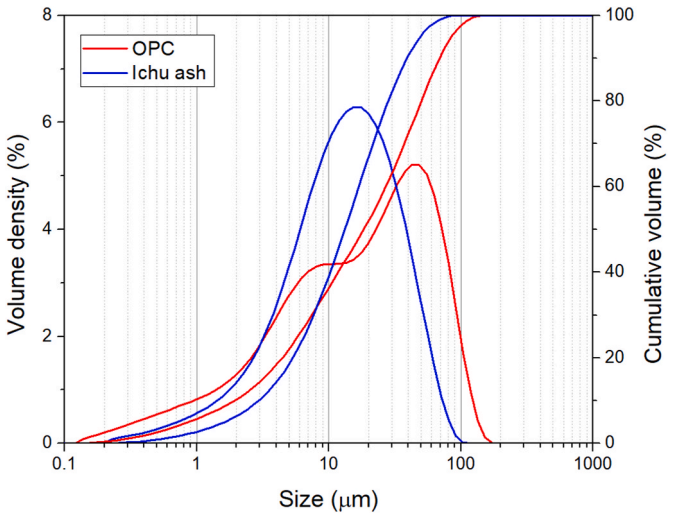

Fig. 1. Particle size distribution of the starting materials.

potentiometric titrator fitted with a combined silver electrode. The chloride content is expressed as a percentage by dry mass of mortar, and the depth assigned to each sample was considered as the midpoint of the depth range at which the sample was collected.

The resistance to chloride transport was evaluated by determining the non-steady state diffusion coefficient (Dnss), which was calculated by fitting the experimental chloride profile to equation (1):

$$C_x = C_i + (C_s + C_i)\left(1 - \mathrm{erf}\left[\frac{x}{2\sqrt{D_{nss}t}}\right]\right) \quad (1)$$

Where C_x represents the chloride concentration measured at depth x and time t, C_i stands for the initial chloride content and C_s for the chloride content at the exposed surface. The experimental value obtained in the uppermost layer was disregarded for the fitting. To compare the results obtained, a one-way ANOVA test was performed, followed by a Tukey HSD post-hoc analysis, at a 95% significance level. All statistical analyses presented in this study were carried out using this methodology.

Additionally, the powder samples extracted from the uppermost and innermost layer of each type of mortar were analysed by thermogravimetry. Regarding the fourth sub-specimen tested, several mortar portions were extracted from it to be examined by X-ray microfluorescence, mercury intrusion porosimetry and computed axial tomography.

2.2.2. Evaluation of carbonation resistance

The carbonation behaviour was assessed in accordance with the procedure described in EN 12390-12 standard [41]. A set comprising three 4x4x16 cm^3 prismatic mortar specimens was prepared for each type of mortar and age tested. The specimens were cured by water immersion for 28 days, and then they were conditioned in a laboratory air environment for 14 days. Afterwards, they were tested in a climatic chamber at 20 °C, 65% R.H. and 3% CO_2 concentration for 0, 28, 70, 130 and 250 days. For each exposure time and type of mortar, two specimens were subjected to flexural and compressive strength tests and their carbonation front was determined on the freshly broken surface by application of a phenolphthalein solution. Pieces representative of the cross-section were taken from the broken specimens, which, after being ground and dried, were tested by thermogravimetry. In addition, a third specimen was tested according to the Spanish standard UNE 83980 [42] to calculate its density and accessible porosity.

As an indirect indicator of the resistance to carbonation, the oxygen permeability of the mortars was studied according to the Spanish standard UNE 83981 [43]. The measurements were carried out in a Cembureau apparatus in a room at controlled temperature (20 ± 2 °C) and relative humidity (50 ± 5%). For this purpose, three mortar discs were used for each type of formulation, each of 5 cm in height and 15 cm in diameter, obtained from cylindrical mortar specimens of 15 cm in diameter and height, cured for 28 days. Prior to the gas permeability test, the specimens were conditioned according to the Spanish standard UNE 83966 [44] in order to have a homogeneous distribution of moisture inside the specimens between 65% and 75%.

2.2.3. Instrumental techniques

The chemical composition of the starting materials was quantified on a Bruker S4 PIONEER X-ray fluorescence spectrometer equipped with a Rh X-ray tube.

The granulometry of the starting materials was measured by laser diffraction using a Mastersizer 3000 particle size analyser equipped with the dry powder dispersion unit Aero S, which presents a measurement range between 0.01 and 3500 μm.

Compressive strength of the mortar specimens was determined on a CONTROLS AUTOMAX model 65-L28D12 test frame.

The thermogravimetric analyses (TG/DTG) were performed on a TA SAT 1600 analyser at a heating rate of 10 °C/min, between 20 °C and 1000 °C, while maintaining an inert atmosphere using nitrogen. The quantification of portlandite, calcite and Friedel's salt concentrations was conducted using the tangential method [45]. The concentration of Friedel's salt (C_{Fs}) was calculated applying equation (2):

$$C_{Fs} = \frac{M_{Fs}}{6 \cdot M_{H_2O}} m_{Fs} \quad (2)$$

Where m_{Fs} represents the mass loss centred at 300 °C, calculated by the tangential method and M_{Fs} and M_{H2O} are the molar masses of Friedel's salt and water, respectively.

The concentration of chloride ions bound as Friedel's salt ($C_{Cl,Fs}$) was determined as follows:

$$C_{Cl,\,Fs} = \frac{C_{Fs} \cdot 2}{M_{Fs}} M_{Cl} \quad (3)$$

Where M_{Cl} is the atomic weight of chlorine.

X-ray microfluorescence (μXRF) was carried out on a Bruker M4 TORNADO instrument fitted with a Rh target and a dual 30 mm^2 silicon drift detector energy dispersive spectrometer (SDD-EDS). Samples were measured under vacuum conditions of 20 mbars using a step size of 10 μm and a dwell time of 10 ms per pixel.

Porosity was evaluated by mercury intrusion porosimetry using a Micromeritics AutoPore IV porosimeter. The instrument is suitable for working with pressures up to 227.5 MPa, achieving a measuring range between 0.006 and 175 μm.

X-ray computed tomography imaging (CT) was obtained on a Nikon XT-H-160 scanner, equipped with a 160 kV W target and a 0.25 mm Cu filter. 1000 scans per sample were recorded, at 4 frames per scan.

3. Results and discussion

3.1. Carbonation resistance

3.1.1. Initial physical properties

Table 2 summarises the properties of the unexposed mortars after 28

Table 2
Properties of non-carbonated mortars after 28 days of water curing and subsequent conditioning (uncertainty expressed as ± one standard deviation).

	OPC	ICHU6	ICHU10
Accessible porosity (%)	13.2	13.4	14.6
Bulk density (g/cm^3)	2.19	2.15	2.10
Compressive strength (MPa)	68.4 ± 1.0	62.8 ± 1.0	52.3 ± 0.2
Oxygen permeability coefficient (k) (m^2)	(1.05 ± 0.22)·10^{-17}	(0.80 ± 0.11)·10^{-17}	(0.79 ± 0.06)·10^{-17}

days of water immersion curing, followed by the conditioning treatment according to the corresponding standard applied (see section 2). As the data indicate, using ichu ash as pozzolan increases the accessible porosity of the specimens, almost imperceptibly for ICHU6 mortar, but more noticeably for ICHU10 mortar (about 10%) with respect to OPC mortar. This effect leads to a decrease in bulk density, which in turn results in a considerable loss of mechanical performance, as evidenced by the compressive strength values in the table. This drop in strength was observed in previous studies [36], which attributed this phenomenon mainly to inhibited portlandite dissolution due to the high levels of alkalis in the ash, as well as to increased macropore formation caused by workability loss.

In contrast, the addition of ichu ash presents benefits in terms of gas permeability, causing a reduction in the oxygen permeability coefficient of about 25% for both ICHU6 and ICHU10 mortars with respect to OPC mortar. Such behaviour is associated with the refinement of the pore network and its lower connectivity (see section 3.2.3). It should be noted that this decrease in gas permeability is substantially higher than for other materials such as ceramic waste (for which a 5% decline is obtained with respect to conventional cement at a 10% substitution level) [46] or slags (21% decrease compared to conventional cement, at a 30% substitution level) [47]. This enhanced decrease in gas permeability is closely related to the intrinsic properties of this new SCM [36], which presents a higher lime-fixing capacity (pozzolanic activity) at short ages than ceramic-based pozzolans and slags.

3.1.2. Carbonation depths

Fig. 2 shows the carbonation front of mortar specimens revealed at different exposure ages by applying phenolphthalein solution to their cross-section. It is evident from the figure that the use of ichu ash adds to the susceptibility to carbonation of the mortars as the percentage of cement substitution increases. As a result, small signs of carbonation can already be detected at some of the edges of ICHU10 mortars after 28 days of exposure. The carbonated areas spread swiftly so that by the end of the experiment more than half of the cross-section is affected by carbonation. In contrast, OPC and ICHU6 mortars display better behaviour, presenting only minor signs of carbonation at 70 days. After 130 days of exposure, the carbonation depth becomes more evident, with a slightly deeper front for ICHU6 mortar. In any case, the carbonated areas are significantly smaller than those registered for ICHU10 mortar. Another significant aspect of ichu blended mortars is that they seem to lead to more uneven carbonation fronts. Such irregularity could be related to the higher porosity and the greater number of macropores linked to ichu ash addition, mentioned in the previous section and further explored in section 3.2.3.

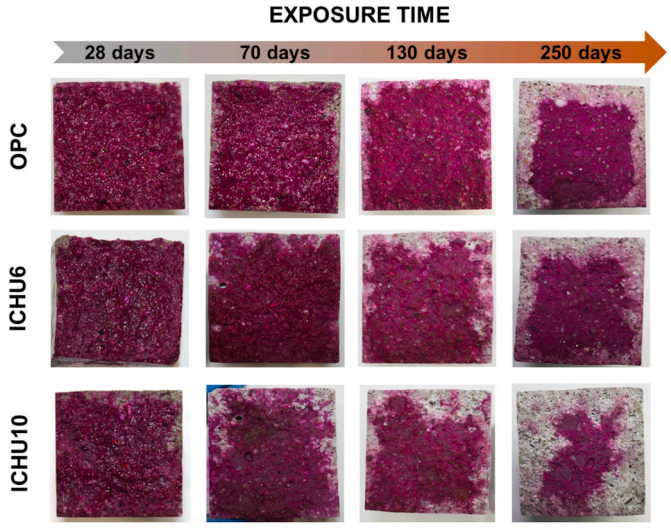

Fig. 2. Evolution of the carbonation front revealed by phenolphthalein spraying.

Fig. 3 compares the relative carbonation depth measured for the mixed mortars with those obtained for the OPC mortar (which are given a value of 1). ICHU6 mortar shows an uneven behaviour throughout the exposure, but it performs similarly to the reference mortar at the end of the experiment. Conversely, ICHU10 specimens exhibit considerably higher values than the rest of the mortars under study, although this difference becomes smaller as exposure progresses. Thus, in the first stages, an almost three-fold increment is observed in the carbonation fronts with respect to those of the reference mortar, but only an increase factor of 1.8 is obtained at 250 days.

The above results contrast with the gas permeability values given in Table 2, from which a higher resistance to the penetration of CO_2 into the matrix could have been predicted for the blended mortars. However, the outcome of the carbonation test is actually not unexpected, since carbonation resistance of cement-based materials often decreases with the addition of supplementary cementitious materials, even though they are likely to develop a more complex microstructure that hinders the penetration of harmful external agents. The reason behind this comes from the reduction in the alkaline reserve due to the consumption of portlandite during the pozzolanic reaction, which facilitates the lowering of the pH by reaction with CO_2 and, therefore, the advance of the carbonation front [48–50]. Among supplementary cementitious materials, biomass-derived pozzolans are no exception. Thus, examples of increased susceptibility to carbonation due to the use of pozzolans of this nature, such as rice husk ash [51–58], sugarcane bagasse ash [59] or palm oil fuel ash [60], are readily available in the literature. The increases in carbonation depth obtained for ichu ash blended mortars in this study are comparable in magnitude to those observed when using the aforementioned vegetable ashes in similar tests.

3.1.3. Evolution of the mineralogical phases by TG/DTG

Given the conflicting data between the carbonation fronts and the oxygen permeability coefficients seen above, the evaluation of the chemistry of the mortars takes centre stage in accounting for their behaviour under CO_2 exposure. The study was carried out by thermogravimetric analysis, given that it is a very convenient technique to identify and quantify the main actors in the carbonation reaction (portlandite and calcium carbonate).

Fig. 4a represents the derivative of the mass loss curves (DTG) of the mortars before the start of the carbonation test. Qualitatively, the three mortars exhibit analogous DTG curves, consisting of mass losses centred at identical temperatures, and therefore attributable to the same compounds. Firstly, a peak at 50 °C can be detected, ascribable to the loss of moisture. The signal at 85 °C is indicative of the dehydration of

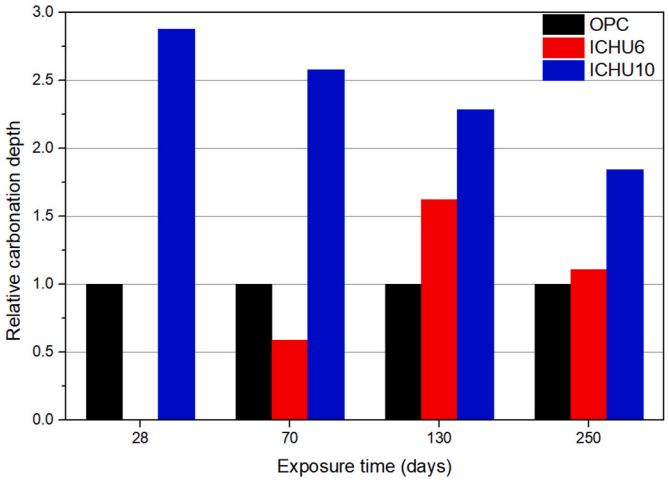

Fig. 3. Evolution of carbonation depth relative to that of OPC mortar.

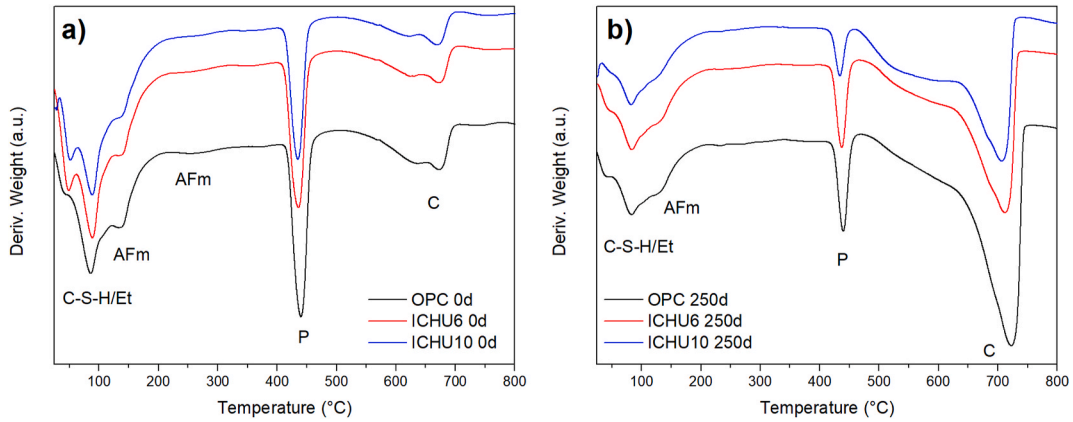

Fig. 4. Differential thermogravimetric curves of the mortars a) before initiating the carbonation test and b) after 250 days of exposure. Et: ettringite, P: portlandite, C: calcium carbonate.

ettringite and C–S–H gels. The peak at 140 °C, together with the broad signal at 260 °C, denotes the presence of AFm phases, as they correspond to the loss of water molecules in the interlayer region and the octahedral layers of this type of compounds, respectively [45]. Their position and the presence of carbonates (probably sourced from the calcite typically contained in Portland as a minority component in cements and evidenced by the weight loss in the 550–700 °C range) suggest that the AFm compounds present in these mortars are likely to be carboaluminates [61,62]. Lastly, the characteristic loss due to the dehydroxylation of portlandite is observed between 400 and 500 °C. The concentration of portlandite in the mortars was quantified, and the results are given in Table 3. These values evidence the pozzolanic effect of ichu ash, as reductions in portlandite concentration of 12% and 29% are obtained for the ICHU6 and ICHU10 mortars, respectively, compared to the OPC mortar, which are too high to be attributed solely to cement dilution effect. This reduction in the initial portlandite content, particularly in the ICHU10 mortar, would be in line with its greater susceptibility to carbonation, owing to its lower initial alkaline reserve.

Exposure to CO_2 leads to a modification of all DTG signals, as can be seen in Fig. 4b, which corresponds to the analysis of the mortars at the end of the experiment. As expected, all mortars experience a decrease in the intensity of the portlandite signal as a consequence of its reaction with CO_2. Proportionally, OPC and ICHU6 mortars present nearly the same reduction in portlandite concentration with respect to the initial one (about 60%, see Table 3). On the other hand, this reduction is considerably greater for ICHU10 mortar, which is consistent with the revealed carbonation depths shown in Fig. 2. As a product of the reaction, calcium carbonate precipitates, which is also confirmed in the DTG curves by the increase of the signal in the 500–750 °C range. According to Table 3, the highest amount of calcium carbonate is produced in OPC mortar, despite presenting the smallest carbonated area. This is because this mortar possesses the largest initial amount of portlandite. Thus, the amount of $CaCO_3$ formed in ICHU6 mortar is considerably lower than that of the OPC despite having similar carbonation depths, as its starting portlandite reserve is smaller. In contrast, the amount of newly formed calcium carbonate increases in the ICHU10 mortar for the opposite reason: it contains a lower initial amount of portlandite susceptible to react with CO_2, but a larger area affected by carbonation.

Table 3
Mass loss between 50 and 300 °C, and concentration of portlandite and calcium carbonate in mortars subjected to the accelerated carbonation test.

	Mass loss 50–300 °C		Portlandite content (%)		$CaCO_3$ content (%)	
	0 days	250 days	0 days	250 days	0 days	250 days
OPC	3.7	2.6	3.5	1.4	1.8	9.0
ICHU6	4.3	2.7	3.1	1.3	1.5	7.1
ICHU10	4.2	2.3	2.5	0.6	1.2	7.3

In addition to the amount of $CaCO_3$ formed, the shape of the DTG peak itself is a matter of interest. A comparison between Fig. 4a and b reveals that the mass loss of carbonates in Fig. 4b is extended towards lower temperatures, giving rise to a broad secondary signal between 500 and 650 °C. This phenomenon is known to be associated with the formation of poorly-crystalline $CaCO_3$, which is in turn linked to the carbonation of C–S–H gels, ettringite and/or AFm phases [63–67]. Indeed, it can be seen that the mass loss is considerably reduced in the 50–300 °C region of the carbonated mortars (see Table 3), and that both the signals corresponding to the C–S–H gels and the AFm phases are reduced. Although both phenomena (extension of the carbonate signal at lower temperatures and reduction of mass loss in the 50–300 °C range) are present in all three mortars under study, the effect is more pronounced in ICHU10 mortar. This can be explained by the fact that the lower availability of portlandite due to its consumption by the pozzolanic reaction renders the remaining phases more susceptible to CO_2 attack. This is of great consequence since the effect of carbonation on the physical properties of materials depends to a large extent on the type of phase affected by the exposure [68,69].

3.1.4. *Effect of carbonation on the physical properties*

Fig. 5a represents the variation of the bulk density of the mortars with exposure time. ICHU6 and ICHU10 mortars experience a general increase in bulk density when exposed to CO_2 action, which is particularly pronounced in the first stage of the test (0–28 days). A slower and subtler variation in bulk density is found for OPC mortar, ultimately also tending to an overall gain. This is consistent with the carbonation reaction of portlandite (slower in OPC mortar), which entails an increase in the solid mass due to the uptake of CO_2 from the environment, leading to the precipitation of calcite, of higher molecular weight.

Carbonation of portlandite is also related to an increase in the volume of solids, and therefore it often leads to a decrease in the porosity of carbonated cement-based materials [66,70,71]. According to Fig. 5b, however, this decrease is not observed over the entire exposure period for the mortars under study, as two distinct stages can be identified: i) an initial phase in which the accessible porosity drops, likely associated with portlandite carbonation, as it is initially the most susceptible phase [66,68] and ii) a second phase in which the porosity rises.

Increased porosity is a common outcome at advanced carbonation stages, which has been both observed by experimental results and predicted by thermodynamic calculations in the literature [63,69,72]. When portlandite availability is reduced, other phases such as ettringite, AFm phases or C–S–H gels are typically affected by CO_2 exposure. In addition to calcite, the carbonation of ettringite leads to the precipitation of gypsum and amorphous alumina, causing a decrease in volume [73–75]. In the case of C–S–H carbonation, a similar situation occurs, as

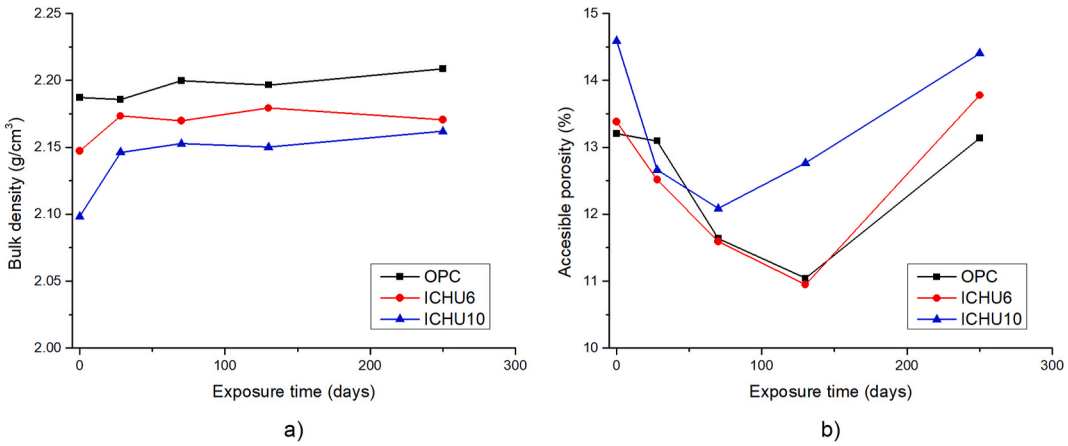

Fig. 5. Variation over time of a) bulk density and b) accessible porosity of the mortars subjected to the accelerated carbonation test.

they initially decalcify generating lower Ca/Si ratio gels and then decarbonate in conjunction with carboaluminates, yielding strätlingite, but upon severe carbonation, they degrade to amorphous silica [68,72,76,77]. As seen previously in Fig. 4b, all mortars experience the carbonation of ettringite, monocarboaluminate and/or C–S–H gels at the end of the experiment, and therefore the existence of the second stage at advanced ages of exposure in Fig. 5a, in which porosity is increased, would be justified by this effect.

The timing at which the increase in porosity occurs is also of interest: whereas OPC and ICHU6 mortars behave almost in a parallel way, showing only an increase in accessible porosity at the end of the experiment (250 days), this change occurs much earlier for ICHU10 mortar, becoming already evident in the 130-day carbonated sample. This delay in the onset of porosity increase is indicative of the predominance of the carbonation of components different from portlandite in ICHU10 mortar. As CO_2 reacts preferentially with portlandite, the mortars with higher portlandite reserves (OPC and ICHU6) offer better protection of the phases whose carbonation has a more detrimental effect on the physical properties of the mortars, which would explain their longer delay in the accessible porosity increase. For this reason, the increase in porosity during carbonation is a phenomenon that is not uncommon in cements containing SCMs [66,70,72].

Regarding the mechanical properties, all mortars subjected to the action of CO_2 experienced an overall increase in compressive strength, as shown in Fig. 6. In the case of OPC mortar, this gain in strength is not discernible until the end of the experiment, as the only statistically significant variation in compressive strength with respect to the starting value (exposure time = 0) is obtained at 250 days of exposure [ANOVA, $F(4,10) = 28.484$, $p < 0.001$; Tukey HSD, $p = 0.001$], where an increase of 20% is observed. Conversely, the gain in strength is already statistically relevant at early stages (28 days) for the ichu-blended mortars [ICHU6: ANOVA, $F(4,10) = 27.637$, $p < 0.001$; Tukey HSD, $p = 0.012$/ ICHU10: ANOVA, $F(4,10) = 32.048$, $p < 0.001$; Tukey HSD, $p = 0.007$]. Compressive strength remains constant thereafter, resulting in no further statistically significant variation until 250 days of exposure, where an increase of 24% and 37% can be observed, respectively, for ICHU6 [Tukey HSD, $p = 0.001$] and ICHU10 [Tukey HSD, $p = 0.028$] mortars. Thus, as the exposure time progresses, the loss of mechanical strength due to the addition of ichu ash is reduced, particularly for ICHU10 mortar, whose loss of mechanical strength relative to OPC mortar descends from 24% at the beginning of the experiment to 12% at the end of the exposure. Accordingly, in terms of mechanical performance, the ichu-blended specimens benefit from the effect of carbonation. It should also be noted that the evolution of the compressive strength follows a trend that resembles that observed for the bulk density, which is to be expected, due to the gain in solid volume from carbonation [77,78].

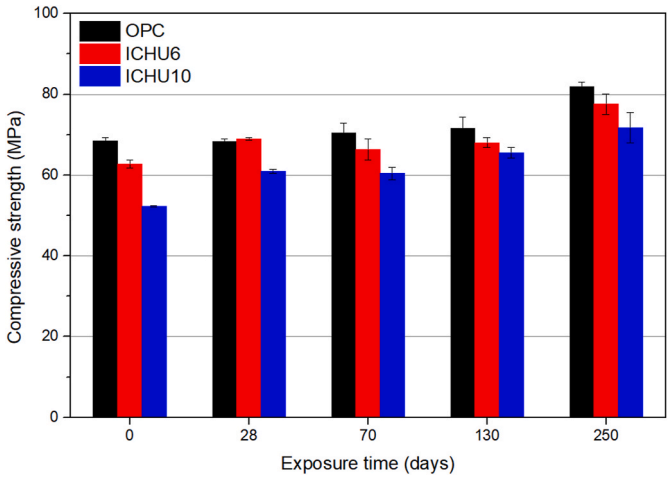

Fig. 6. Evolution of compressive strength over time of the specimens exposed to the accelerated carbonation test.

The results obtained indicate that the mortars containing ichu ash exhibit a behaviour with respect to carbonation that is in line with the performance typically found for pozzolans in general, and in particular for those derived from vegetable ashes. Therefore, it is to be expected that ichu ash blended mortars will display the same limitations in terms of applications involving steel reinforcement in environments where corrosion is likely to occur (XC1-XC4 exposure classes), for which only low replacement levels could be admissible. Conversely, these new materials could be suitable for uses where reinforcement is not required or where the risk of corrosion is low, as carbonation was found to have no negative effect on their physical properties and even improved them in some aspects. In any case, it is important to note that the findings were obtained by an accelerated carbonation method. Natural carbonation tests, reflecting the actual conditions of use, should therefore be carried out before real applications are taken into consideration. Moreover, considering that the most efficient use of this resource in economic, social and environmental terms would be local exploitation, the selected study conditions should reflect the climate of the regions where ichu grass can be harvested. This is of paramount importance as temperature and, especially, humidity conditions can have dramatic consequences on carbonation, particularly for pozzolanic materials, which promote the refinement of the porous structure and, therefore, favour its saturation with water under the appropriate conditions, thus potentially preventing the advance of carbonation.

3.2. Chloride resistance

3.2.1. Chloride mapping and profiling

The spatial distribution of the chloride ions in the mortars, arising from their diffusion during the ponding test, was qualitatively observed by μXRF mapping at the end of the experiment. The results, shown in Fig. 7, reveal that chloride ion ingress occurs faster in the OPC mortar than in those including ichu ash as pozzolan, thus reaching greater penetration depths. In contrast, ICHU6 and ICHU10 mortars (which behave similarly) favour the accumulation of chloride ions in the upper strata, delaying their advance.

Fig. 8 presents the average chloride profiles for each type of mortar under study. As can be seen, only minor differences are perceived between the addition of ichu ash at 6% and 10% replacement levels, yielding nearly equivalent chloride profiles. Compared to that of OPC mortar, ICHU6 and ICHU10 mortars exhibit a steeper profile, where chloride ions reach shallower depths (their concentration is practically nil after 10 mm depth), yet they accumulate more in the near-surface layers. Consequently, the results are consistent with the elemental maps previously seen in Fig. 7, verifying that the addition of ichu ash has the effect of hindering the advance of chloride ions.

To quantify the extent of the delay in the chloride ingress provoked by the pozzolan, the non-steady state diffusion coefficient (D_{nss}) was calculated by adjusting the experimental chloride profiles to equation (1). An excellent fit was achieved, as evidenced by the R^2 values given in Table 4, where the best-fit parameters are also reported. No statistical difference was found for the values found for mortars ICHU6 and ICHU10 (ANOVA $F(2,6) = 48.433$, $p < 0.001$; Tukey HSD, $p = 0.900$), for which a reduction of approximately 60% in the diffusion coefficient was obtained with respect to that of OPC mortar, and an increase in the accumulation of chloride ions on the surface by ca. 20%.

These findings are in agreement with the literature, in which it is widely acknowledged that the use of supplementary cementitious materials (including some vegetable ashes such as rice husk ash [51,79–86], bagasse ash [80,87,88], palm oil fuel ash [89–91] or bamboo leaf ash [92]) tends to reduce chloride permeability [90,93–96]. According to the literature, ichu ash seems to be more efficient in decreasing the chloride diffusion coefficient than other common vegetable ashes. More specifically, the use of rice husk ash and bagasse ash at substitution levels equivalent to those in this study tends to result in diffusion coefficients between 5 and 35% lower than those using conventional portland cement [79,84,87,88], although Sousa et al. [81] reported reductions of around 80% for the use of RHA at 10% substitution level. However, it is important to be cautious when comparing these results, as the values in the literature generally derive from accelerated migration tests, rather than from natural diffusion studies, as is the case in this article.

Regarding the means by which pozzolans tend to delay the progress of chloride ions in cement-based matrices, they usually consist of an increase in the chloride binding capacity of the cement paste and/or a decrease in permeability [96,97]. Both aspects will be discussed in the following sections.

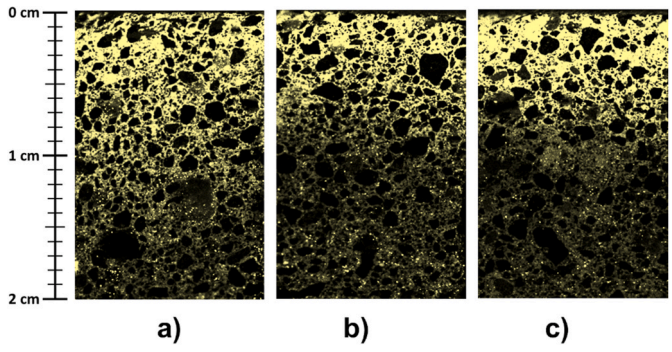

Fig. 7. Elemental maps for Cl in a) OPC, b) ICHU6 and c) ICHU10 mortars (chloride ion ingress from the top).

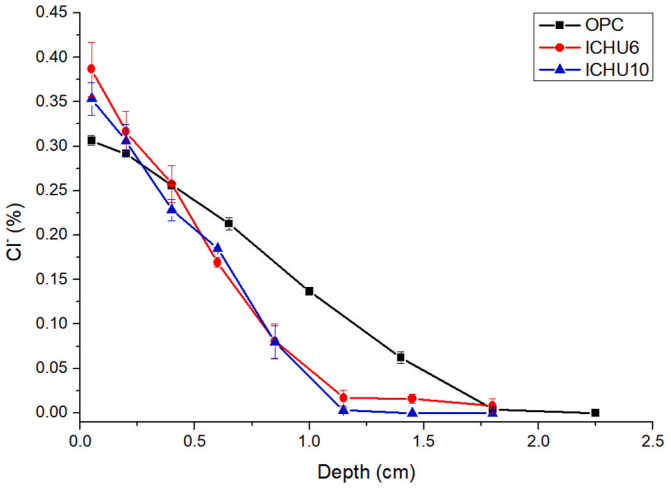

Fig. 8. Chloride profiles obtained after the ponding test (experimental data shows mean values and standard error).

Table 4
Best-fitting parameters obtained from adjusting chloride profiles to equation (1) (uncertainty expressed as ± one standard deviation).

	D_{nss} x 10^{-8} (cm^2/s)	C_s (%)	R^2
OPC	7.1 ± 0.6	0.361 ± 0.01	0.985 ± 0.003
ICHU6	2.9 ± 0.6	0.42 ± 0.07	0.971 ± 0.009
ICHU10	2.9 ± 0.7	0.44 ± 0.08	0.985 ± 0.012

3.2.2. Chloride binding

Fig. 9 depicts the differential thermogravimetric curves of samples taken close to the exposed surface (at an average depth of 2 mm),

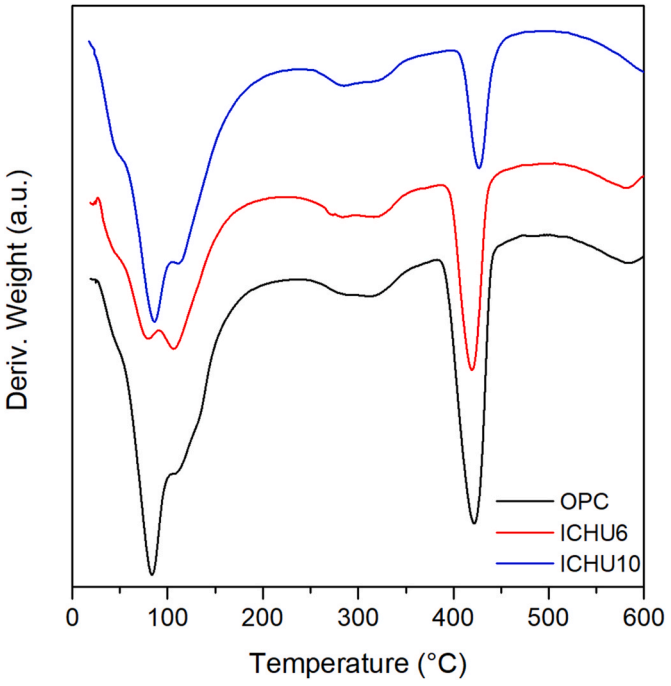

Fig. 9. Derivative of the mass loss curves of the samples taken from the upper layers of the specimens subjected to the ponding test.

collected at the end of the experiment. The curves resemble those of the mortars unexposed to aggressive agents, previously seen in Fig. 4a. Accordingly, all of them preserve the typical mass loss caused by the dehydration of C–S–H gels and ettringite at 85 °C, the characteristic portlandite peak between 400 °C and 450 °C - decreasing in intensity as the percentage of substitution of ichu ash increases- and two mass losses between 100 °C and 350 °C related to the AFm phases. The latter, however, display significant shifts in position with respect to those observed in the unexposed mortars. Firstly, the signal associated with the loss of water from the interlayer in the AFm phases, previously located at 140 °C in chloride-free mortars, is shifted towards lower temperatures, being now positioned at 110 °C. Conversely, the broad signal resulting from the dehydration of the octahedral layers in the AFm phases varies from being centred at 260 °C to covering the 250–350 °C temperature range. Both shifts are consistent with the reaction of chloride ions with carboaluminate-type phases to produce Friedel's salt [63,98,99]. Therefore, these results evidence the chemical binding of chloride ions in the upper strata of all the mortars under study.

Thermogravimetric analysis has proven to be an effective method for quantifying Friedel's salt in mortars and, consequently, for assessing its chemical binding capacity [99,100]. Accordingly, the concentration of Friedel's salt (C_{Fs}) was calculated applying equation (2), leading to the results reported in Table 5. Apparently, these results do not reveal a clear trend between the proportion of ichu ash added and the Friedel's salt formed, as the highest amounts of Friedel's salt are obtained in the ICHU6 mortar. It should be remembered, however, that the concentration of chloride ions accumulated in the superficial layers of the mortars differs according to the type of cement used (see Fig. 8), which dictates the extent to which Friedel's salt is produced. Therefore, to obtain comparable results, the amount of chloride ions retained as Friedel's salt ($C_{Cl,Fs}$) was calculated for each type of mortar using equation (3), which was subsequently used to calculate their ratio with respect to the corresponding surface chloride concentration (C_s). The results obtained are shown in Table 5, where it can be seen that, proportionally, the addition of ichu ash tends to mitigate the retention of chlorides as Friedel's salt. This mitigation is very slight for the ICHU6 mortar, but more noticeable for the ICHU10 mortar, in which a reduction of approximately one third of the value observed for the OPC is reached.

These results are justifiable by the fact that the addition of a silicon-based SCM, such as ichu ash, dilutes the amount of aluminium-rich compounds in the cement, thus decreasing its potential for the precipitation of AFm phases, including Friedel's salt [101,102]. Nevertheless, it should be highlighted that Friedel's salt formation is not the only binding mechanism for chloride ions in cement-based matrices, as they can also be physically bound by being adsorbed in C–S–H gels. However, it seems unlikely that the use of ichu ash could positively contribute to chloride ion binding by this mechanism since chloride ion adsorption is usually enhanced by high C/S ratios in C–S–H gels [101,103–105], which would not be expected in this case due to the high silica content of ichu ash. Both factors (reduction of the alumina content and the C/S ratio in C–S–H gels) have been reported to be responsible for the decline in chloride binding in other silica-rich pozzolans, like silica fume [101,103,106].

Based on the results presented in this section, the improvement in the resistance to chloride ions penetration observed with the addition of ichu ash cannot be attributed to the effect of the pozzolan on chloride binding, as it occurs in other similar SCMs, such as the aforementioned silica fume.

Table 5
Concentration of Friedel's salt and chemically bound chlorides at an average depth of 2 mm.

	C_{Fs} (%)	$C_{Cl,Fs}$ (%)	$C_{Cl,Fs}/C_s$
OPC	1.1	0.14	0.39
ICHU6	1.3	0.16	0.38
ICHU10	0.9	0.11	0.26

3.2.3. Pore network characterisation

The pore network characteristics of the mortars were examined by analysing samples taken from the unaffected area by mercury intrusion porosimetry. The resulting pore distribution curves are shown in Fig. 10, whereas Table 6 lists the measured porosity and average pore size of each mortar. Similarly to what was observed in section 3.1.1 concerning accessible porosity, OPC and ICHU6 mortars exhibit identical values of MIP-measured porosity. Also following the aforementioned trend, porosity increases for ICHU10 mortar (by approximately 3% in this case, with respect to OPC and ICHU6 values). Regarding pore size, OPC and ICHU6 pore distribution curves present similar shapes, both peaking around 0.1 μm at comparable intensities. ICHU6 distribution curve, however, is slightly shifted towards smaller pore diameters, leading to a decrease in the average pore size of ca. 30% compared to that of OPC. This effect is more pronounced for ICHU10 mortar, where, in addition to the shift of the curve towards smaller sizes, a significant decrease in the proportion of pores around 0.1 μm is detected, accompanied by a large increase in the proportion of pores below 0.05 μm. In addition, substantial growth in the proportion of larger pores (above 0.5 μm) can also be found. In spite of this, the average pore size decreases even further than for ICHU6 mortar, giving rise to a 43% reduction compared to OPC mortar.

Macroporosity was further studied by computed axial tomography (CAT) on 2.5 cm high samples taken from the exposed area of the specimens, producing the results depicted in Figs. 11 and 12. A general growth in the number of macropores can be seen as the substitution by ichu ash becomes higher, reaching more than twice the number of pores in the case of ICHU10 compared to OPC. Nevertheless, as found in the MIP tests and as seen in Fig. 12a, even though there is a growing number of pores, the proportion of larger pores decreases in favour of smaller ones, particularly for ICHU10 mortar.

Both techniques (MIP and CT) confirm that, although porosity may be enhanced, the addition of ichu ash results in further refinement and increased complexity of the pore network. This is a common phenomenon in blended cements, triggered by the precipitation of secondary hydration products derived from the pozzolanic reaction in the voids originally generated by cement hydration, which is typically associated with a decrease in the permeability and ionic diffusion of the material [48,107]. Such an increase in the complexity of the microstructure is considered to be one of the main causes of improved durability in blended cements, particularly concerning the resistance to chloride ion transport. In fact, some authors even consider that the refinement of the pore network and its increase in tortuosity are the most influential

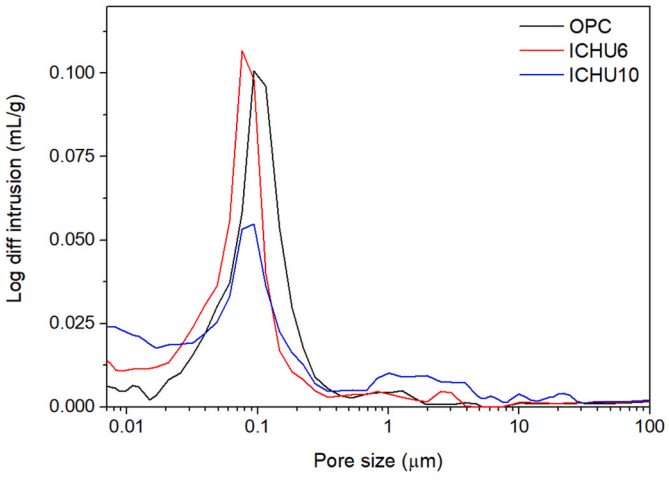

Fig. 10. MIP pore size distribution of samples extracted from the unexposed regions of the specimens subjected to the chloride ponding test.

Table 6
Pore network properties of the unaffected region of the mortars, measured by mercury intrusion porosimetry at the end of the experiment.

	Porosity (%)	Average pore size (μm)
OPC	11.9	0.067
ICHU6	11.9	0.046
ICHU10	12.3	0.038

parameters on the resistance to chloride diffusion, even above their chloride binding capacity [100,108]. In this regard, it should be noted that previous studies with ichu ash have shown not only that this kind of pozzolan prompted the refinement of the microstructure of the blended mortars, but also that it reduced their sorptivity and increased their resistivity, evidencing lower pore connectivity, greater tortuosity of the pore network and, in essence, lower permeability [36]. It must also be pointed out that there is a well-known inverse relationship between resistivity and chloride ion diffusion coefficients [109–112]. Considering that the aforementioned studies [36] showed significant increases in resistivity due to the addition of ichu ash (up to 4 times higher than that of OPC at 90 days of curing for ICHU10) it would be expected that this parameter, and therefore pore size and connectivity, would be of great relevance in the transport of chlorides for the mortars under study. This is also in agreement with the literature on pozzolans derived from vegetable ashes, where their enhanced resistance to chloride penetration is frequently attributed to their effect on the microstructure, and it often appears in conjunction with a reduction in sorptivity and an increase in resistivity [80,81,84,85,87,90,91,113,114].

The modification of the pore network due to the precipitation of Friedel's salt crystals is another aspect that can alter the transport of chloride ions during the experiment. This effect was also studied by CT, since crystallisation in larger pores is usually favoured [115–117], and because this technique facilitates the study of the microstructure at different depths. To perform the analysis, the samples were divided into three regions: i) an outer region comprising the most exposed layers (0–5 mm); ii) an intermediate region (5–15 mm); and iii) an internal zone, marginally altered by the exposure (15–25 mm). The distribution according to the number of pores, as well as the average pore volume, is shown in Fig. 12b. Firstly, as previously seen in Fig. 12a, the addition of ichu ash leads to a decrease in the proportion of larger pores in all the layers, favouring the formation of finer pores and thereby inducing a significant reduction in their average pore volume. A comparison of the three layers in each mortar type reveals that all mortars feature a finer pore distribution in the outer strata than in the inner ones, as expected from the precipitation of chloride-containing phases. This behaviour, however, differs slightly depending on the type of mortar. OPC mortar exhibits a reduction in the average pore size in the superficial area of approximately 15% with respect to that of the internal area, which also spreads to the intermediate area (as expected, given that OPC is the material where further advance of chlorides occurs), to a similar extent. ICHU6 mortar shows a higher degree of refinement, in the order of 30% in the average pore volume, although only observable in the outer layer. Nevertheless, the largest decline in pore volume is found for ICHU10 mortar, with reductions of approximately 45% and 35% in the upper and intermediate layers, respectively, compared to the core. The superior degree of refinement in the upper strata of ICHU6 and ICHU10 mortars could be explained by the enhanced accumulation of chloride ions close to the surface in these specimens (see Table 5). In addition, a finer and more complex initial microstructure could improve the efficiency of the

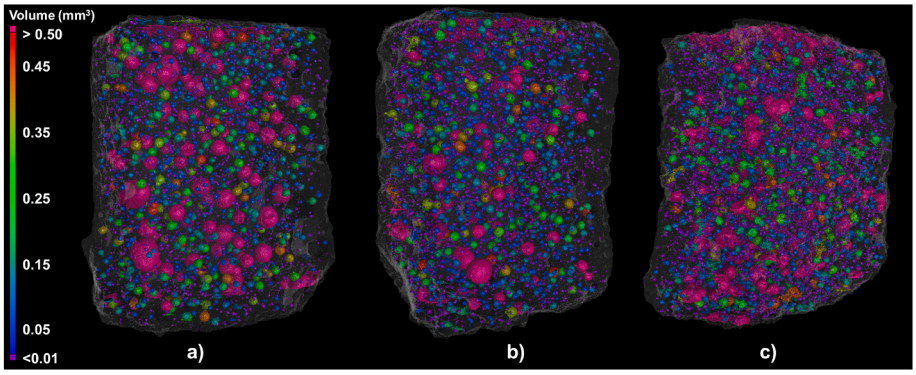

Fig. 11. Macropore distribution in a) OPC, b) ICHU6 and c) ICHU10 samples measured by CT scanning (chloride ion ingress from the top).

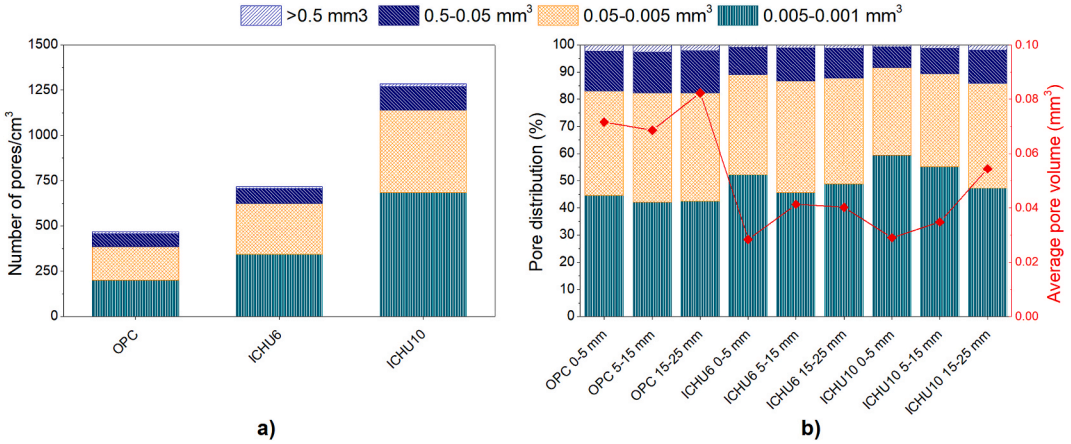

Fig. 12. a) Number of pores in the mortars and b) pore distribution (by number of pores) and average pore volume of the different regions of the mortars assessed by CT scanning.

additional refinement caused by the exposure to chloride ions.

In view of the results obtained, the greater delay in the advance of chloride ions in the blended mortars mainly originates from the refinement of their microstructure by the pozzolanic effect. Moreover, their higher complexity and tortuosity cause blended mortars to become more effectively further refined as chloride ions advance into the matrix and crystallise to form compounds such as Friedel's salt. This second type of refinement, however, is limited by the chloride binding capacity of the cement, which, as discussed in section 3.2.2, becomes more limited as the ichu ash substitution level increases. This is probably why the chloride diffusion coefficient of ICHU10 mortar is not significantly higher than that of ICHU6 mortar, despite presenting a more complex microstructure.

Consequently, ichu ash presents interesting properties in terms of reducing the penetration of chloride ions in cement-based materials, which is of great interest to prevent the corrosion of reinforcement in chloride-rich environments. It should be noted, however, that even though the rate of chloride diffusion is a key aspect in this matter, other factors should also be taken into account. In particular, the critical chloride content, above which steel corrosion begins, can also be influenced by the addition of pozzolans. Pozzolans often negatively affect this aspect by reducing the alkaline reserve, which frequently results in a decrease in the critical chloride content [118–120]. However, it is difficult to make predictions for ichu ash, especially considering its high alkali content. It is, therefore, necessary to consider future studies that include corrosion tests and critical chloride content analyses.

4. Conclusions

The conclusions that can be drawn from this work can be summarised as follows:

1. Mortars prepared by cements containing 6% and 10% of ichu ash (ICHU6 and ICHU10) are distinguished by a larger volume of macropores, which leads to reduced density and mechanical strength values. However, it also provides them with a more complex microstructure, reducing the rate at which fluids penetrate the mortars. This effect is more pronounced for ICHU10 mortars.
2. Regarding carbonation resistance, a reduction is observed with the addition of ichu ash, leading to faster carbonation rates than that of OPC mortar. Only a minor increase is detected for ICHU6 specimens, but it becomes substantially higher for ICHU10 mortar. The reason for this was found primarily in the reduction of the portlandite reserve that takes place as the amount of ichu ash increases, a common phenomenon among pozzolans. As a consequence, a noticeable increase in the carbonation of ettringite, carboaluminates and C–S–H gels is experienced by ICH10 mortars. Despite this, all mortars under study exhibit an increase in their mechanical properties and bulk density.
3. The addition of ichu ash as a pozzolan has a significant positive effect on the resistance to chloride penetration, as it reduces the non-steady state diffusion coefficient by 60% with respect to OPC mortar, for both ICHU6 and ICHU10 mortars. It was found that this improvement is primarily related to the refinement of the pore network in ichu-blended mortars, rather than to their chloride binding ability.

Hence, the utilisation of ichu ash as supplementary cementitious material shows potential for the production of durable and sustainable cement-based materials, although its implementation at replacement percentages of 10% would be discouraged for those applications where carbonation could be a concern (XC1-XC4 exposure classes). In any event, further research is required to gain a deeper understanding of the durable properties of this material, either by further exploring the durable properties studied in this work (carbonation tests in natural environments, corrosion analysis, etc.) or by analysing other deterioration processes. In particular, studies related to the alkali-silica reaction would be of special interest, as the combination of the high amorphous silica and K_2O contents of the ichu ash could be a potential source of concern in this regard.

Declaration of competing interest

The authors declare that they have no known competing financial interests or personal relationships that could have appeared to influence the work reported in this paper.

Acknowledgements

This research work was carried out thanks to the Framework Partnership Agreement between CSIC (Spain) and UTEC (Peru) [ref. n. ACAM 2021040044 BDC and 20215065] and the economic support of FONDECYT [contract n. 103-2018-FONDECYT –BM]. L. C-M. gratefully acknowledges the funding received by the Spanish Training Programme and the European Social Fund (MINECO/ESF) [grant number BES-2016-078454]. Funding for open access charge: Universidade da Coruña.

References

[1] T. Gao, L. Shen, M. Shen, L. Liu, F. Chen, Analysis of material flow and consumption in cement production process, J. Clean. Prod. 112 (2016) 553–565, https://doi.org/10.1016/j.jclepro.2015.08.054.
[2] H.G. Van Oss, A.C. Padovani, Cement manufacture and the environment - Part I: chemistry and technology, J. Ind. Ecol. 6 (2002) 89–105, https://doi.org/10.1162/108819802320971650.
[3] M. Schneider, The cement industry on the way to a low-carbon future, Cem. Concr. Res. 124 (2019), 105792, https://doi.org/10.1016/j.cemconres.2019.105792.
[4] S. Supino, O. Malandrino, M. Testa, D. Sica, Sustainability in the EU cement industry: the Italian and German experiences, J. Clean. Prod. 112 (2016) 430–442, https://doi.org/10.1016/j.jclepro.2015.09.022.
[5] M.C.G. Juenger, R. Snellings, S.A. Bernal, Supplementary cementitious materials: new sources, characterization, and performance insights, Cem. Concr. Res. 122 (2019) 257–273, https://doi.org/10.1016/j.cemconres.2019.05.008.
[6] V. Charitha, V.S. Athira, V. Jittin, A. Bahurudeen, P. Nanthagopalan, Use of different agro-waste ashes in concrete for effective upcycling of locally available resources, Constr. Build. Mater. 285 (2021), https://doi.org/10.1016/j.conbuildmat.2021.122851.
[7] F. Martirena, J. Monzó, Vegetable ashes as supplementary cementitious materials, Cem. Concr. Res. 114 (2018) 57–64, https://doi.org/10.1016/j.cemconres.2017.08.015.
[8] R. Rithuparna, V. Jittin, A. Bahurudeen, Influence of different processing methods on the recycling potential of agro-waste ashes for sustainable cement production: a review, J. Clean. Prod. 316 (2021), https://doi.org/10.1016/j.jclepro.2021.128242.
[9] B.S. Thomas, J. Yang, K.H. Mo, J.A. Abdalla, R.A. Hawileh, E. Ariyachandra, Biomass ashes from agricultural wastes as supplementary cementitious materials or aggregate replacement in cement/geopolymer concrete: a comprehensive review, J. Build. Eng. 40 (2021), https://doi.org/10.1016/j.jobe.2021.102332.
[10] S. Luhar, T.W. Cheng, I. Luhar, Incorporation of natural waste from agricultural and aquacultural farming as supplementary materials with green concrete: a review, Compos. Part B Eng. 175 (2019), https://doi.org/10.1016/j.compositesb.2019.107076.
[11] V.S. Vassilev, D. Baxter, L.K. Andersen, C.G. Vassileva, An overview of the composition and application of biomass ash.: Part 2. Potential utilisation, technological and ecological advantages and challenges, Fuel 105 (2013) 19–39.
[12] M.A. Munawar, A.H. Khoja, S.R. Naqvi, M.T. Mehran, M. Hassan, R. Liaquat, U. F. Dawood, Challenges and opportunities in biomass ash management and its utilization in novel applications, Renew. Sustain. Energy Rev. 150 (2021), https://doi.org/10.1016/j.rser.2021.111451.
[13] M. Cabrera, J.L. Díaz-lópez, F. Agrela, J. Rosales, Eco-efficient cement-based materials using biomass bottom ash: a review, Appl. Sci. 10 (2020) 1–23, https://doi.org/10.3390/app10228026.
[14] A.K. James, R.W. Thring, S. Helle, H.S. Ghuman, Ash management review-applications of biomass bottom ash, Energies 5 (2012) 3856–3873, https://doi.org/10.3390/en5103856.
[15] S. Voshell, M. Mäkelä, O. Dahl, A review of biomass ash properties towards treatment and recycling, Renew. Sustain. Energy Rev. 96 (2018) 479–486, https://doi.org/10.1016/j.rser.2018.07.025.
[16] E.Y. Nakanishi, M. Frías, S. Martínez-Ramírez, S.F. Santos, M.S. Rodrigues, O. Rodríguez, H. Savastano, Characterization and properties of elephant grass ashes as supplementary cementing material in pozzolan/$Ca(OH)_2$ pastes, Constr. Build. Mater. 73 (2014) 391–398, https://doi.org/10.1016/j.conbuildmat.2014.09.078.

[17] E.Y. Nakanishi, M. Frías, S.F. Santos, M.S. Rodrigues, R. Vigil De La Villa, O. Rodriguez, H.S. Junior, Investigating the possible usage of elephant grass ash to manufacture the eco-friendly binary cements, J. Clean. Prod. 116 (2016) 236–243, https://doi.org/10.1016/j.jclepro.2015.12.113.

[18] G.C. Cordeiro, C.P. Sales, Pozzolanic activity of elephant grass ash and its influence on the mechanical properties of concrete, Cem. Concr. Compos. 55 (2015) 331–336, https://doi.org/10.1016/j.cemconcomp.2014.09.019.

[19] S. Martínez-Ramírez, M. Frías, E.Y. Nakanishi, H. Savastano, Pozzolanic reaction of a biomass waste as mineral addition to cement based materials: studies by nuclear magnetic resonance (NMR), Int. J. Concr. Struct. Mater. 13 (2019), https://doi.org/10.1186/s40069-019-0342-3.

[20] J. da S. Andrade Neto, M.J.S. de França, N.S. de Amorim Júnior, D.V. Ribeiro, Effects of adding sugarcane bagasse ash on the properties and durability of concrete, Constr. Build. Mater. 266 (2021), https://doi.org/10.1016/j.conbuildmat.2020.120959.

[21] T.A. Santos, R.A. Argolo, D.V. Ribeiro, The effect of the calcination temperature on the physical, chemical and mineralogical characteristics of sugar cane bagasse ash (SCBA) for use as pozzolan, J. Solid Waste Technol. Manag. 47 (2021) 546–556, https://doi.org/10.5276/jswtm/2021.546.

[22] D.V. Ribeiro, M.R. Morelli, Effect of calcination temperature on the pozzolanic activity of Brazilian sugar cane bagasse ash (SCBA), Mater. Res. 17 (2014) 974–981, https://doi.org/10.1590/S1516-14392014005000093.

[23] S.A. Zareei, F. Ameri, N. Bahrami, Microstructure, strength, and durability of eco-friendly concretes containing sugarcane bagasse ash, Constr. Build. Mater. 184 (2018) 258–268, https://doi.org/10.1016/j.conbuildmat.2018.06.153.

[24] E. Villar-Cociña, M. Frias, E.V. Morales, Sugar cane wastes as pozzolanic materials: application of mathematical model, ACI Mater. J. 105 (2008) 258–264.

[25] G.C. Cordeiro, R.D. Toledo Filho, E.M.R. Fairbairn, Effect of calcination temperature on the pozzolanic activity of sugar cane bagasse ash, Constr. Build. Mater. 23 (2009) 3301–3303, https://doi.org/10.1016/J.CONBUILDMAT.2009.02.013.

[26] M. Frías, E. Villar, H. Savastano, Brazilian sugar cane bagasse ashes from the cogeneration industry as active pozzolans for cement manufacture, Cem. Concr. Compos. 33 (2011) 490–496, https://doi.org/10.1016/j.cemconcomp.2011.02.003.

[27] C.J. Prychid, P.J. Rudall, M. Gregory, Systematics and biology of silica bodies in monocotyledons, Bot. Rev. 69 (2003) 377–440, https://doi.org/10.1663/0006-8101(2004)069, 0377, SABOSB]2.0.CO;2.

[28] M.J. Hodson, P.J. White, A. Mead, M.R. Broadley, Phylogenetic variation in the silicon composition of plants, Ann. Bot. 96 (2005) 1027–1046, https://doi.org/10.1093/aob/mci255.

[29] J.F. Ma, N. Yamaji, Silicon uptake and accumulation in higher plants, Trends Plant Sci 11 (2006) 392–397, https://doi.org/10.1016/j.tplants.2006.06.007.

[30] V. Prem Kumar, V. Vasugi, Bamboo materials in cement, geopolymer and reinforced concrete as sustainable solutions for better tomorrow, IOP Conf. Ser. Earth Environ. Sci. 573 (2020), https://doi.org/10.1088/1755-1315/573/1/012036.

[31] E. Aprianti, P. Shafigh, S. Bahri, J.N. Farahani, Supplementary cementitious materials origin from agricultural wastes - a review, Constr. Build. Mater. 74 (2015) 176–187, https://doi.org/10.1016/j.conbuildmat.2014.10.010.

[32] S. Charca, C. Tenazoa, S.J. Holmer, Chemical composition of natural fibers using the measured true density. Case study: ichu fibers, J. Nat. Fibers. (2021), https://doi.org/10.1080/15440478.2021.1952143.

[33] C. Tenazoa, H. Savastano, S. Charca, M. Quintana, E. Flores, The effect of alkali treatment on chemical and physical properties of ichu and cabuya fibers, J. Nat. Fibers. 18 (2021) 923–936, https://doi.org/10.1080/15440478.2019.1675211.

[34] S. Mori, C. Tenazoa, S. Candiotti, E. Flores, S. Charca, Assessment of ichu fibers extraction and their use as reinforcement in composite materials, J. Nat. Fibers. 17 (2020) 700–715, https://doi.org/10.1080/15440478.2018.1527271.

[35] S. Charca, S. Candiotti, Mechanical properties characterization of the Ichu fibers composites, IOP Conf. Ser. Mater. Sci. Eng. 942 (2020), https://doi.org/10.1088/1757-899X/942/1/012010.

[36] M. Frías, L. Caneda-Martínez, M.I. Sánchez de Rojas, C. Tenazoa, E. Flores, Scientific and technical studies on eco-efficient binary cements produced with thermally activated ichu grass: behaviour and properties, Cem. Concr. Compos. 111 (2020), https://doi.org/10.1016/j.cemconcomp.2020.103613.

[37] CEN-CENELEC, European Standard EN 197-1:2011. Cement - Part 1: Composition, specifications and conformity criteria for common cements, Brussels, Belgium, 2011.

[38] CEN-CENELEC, European Standard EN 196-1. Methods of Testing Cement - Part 1: Determination of Strength, Brussels, Belgium, 2018.

[39] CEN-CENELEC, EN 12390-11:2019. Testing Hardened Concrete - Part 11: Determination of the Chloride Resistance of Concrete, unidirectional diffusion, Brussels, Belgium, 2019.

[40] CEN-CENELEC, European Standard EN 14629:2007. Products and Systems for the Protection and Repair of Concrete Structures - Test Methods, Determination of chloride content in hardened concrete, Brussels, Belgium, 2007.

[41] CEN-CENELEC, EN 12390-12:2020. Testing Hardened Concrete - Part 12: Determination of the Carbonation Resistance of Concrete, Accelerated carbonation method, Brussels, Belgium, 2020.

[42] AENOR, UNE 83980:2014, Durabilidad del hormigón. Métodos de ensayo. Determinación de la absorción de agua, la densidad y la porosidad accesible al agua del hormigón, Madrid, Spain, 2014.

[43] AENOR, UNE 83981:2008, Durabilidad del hormigón. Métodos de ensayo, Determinación de la permeabilidad al oxígeno del hormigón endurecido, Madrid, Spain, 2008.

[44] AENOR, UNE 83966:2008, Durabilidad del hormigón. Métodos de ensayo, Acondicionamiento de probetas de hormigón para los ensayos de permeabilidad a gases y capilaridad., Madrid, Spain, 2008.

[45] B. Lothenbach, P. Durdziński, K. De Weerdt, Thermogravimetric analysis, in: K. Scrivener, R. Snellings, B. Lothenbach (Eds.), A Practical Guide to Microstructural Analysis of Cementitious Materials, CRC Press, Boca Raton, 2016, pp. 177–211, https://doi.org/10.1201/b19074.

[46] L. Li, W. Liu, Q. You, M. Chen, Q. Zeng, C. Zhou, M. Zhang, Relationships between microstructure and transport properties in mortar containing recycled ceramic powder, J. Clean. Prod. 263 (2020), https://doi.org/10.1016/j.jclepro.2020.121384.

[47] A. Hadj Sadok, L. Courard, Chloride diffusion and oxygen permeability of mortars with low active blast furnace slag, Constr. Build. Mater. 181 (2018) 319–324, https://doi.org/10.1016/j.conbuildmat.2018.06.036.

[48] M.J. McCarthy, T.D. Dyer, Pozzolanas and pozzolanic materials, in: Lea's Chemistry of Cement and Concrete, fifth ed., 2019, pp. 363–467, https://doi.org/10.1016/b978-0-08-100773-0.00009-5.

[49] W. Ashraf, Carbonation of cement-based materials: challenges and opportunities, Constr. Build. Mater. 120 (2016) 558–570, https://doi.org/10.1016/j.conbuildmat.2016.05.080.

[50] F. Pacheco Torgal, S. Miraldo, J.A. Labrincha, J. De Brito, An overview on concrete carbonation in the context of eco-efficient construction: evaluation, use of SCMs and/or RAC, Constr. Build. Mater. 36 (2012) 141–150, https://doi.org/10.1016/j.conbuildmat.2012.04.066.

[51] J. Wang, J. Xiao, Z. Zhang, K. Han, X. Hu, F. Jiang, Action mechanism of rice husk ash and the effect on main performances of cement-based materials: a review, Constr. Build. Mater. 288 (2021), https://doi.org/10.1016/j.conbuildmat.2021.123068.

[52] B. Chatveera, P. Lertwattanaruk, Durability of conventional concretes containing black rice husk ash, J. Environ. Manage. 92 (2011) 59–66, https://doi.org/10.1016/j.jenvman.2010.08.007.

[53] V. Kumar, S.R. Pandey, A. Kumar, Study of compressive strength of self-compacting concrete using rice husk ash and nano silica as a partial replacement to cement: a comparative study, Lect. Notes Civ. Eng. 135 LNCE (2021) 61–69, https://doi.org/10.1007/978-981-33-6389-2_7.

[54] N. Nisar, J.A. Bhat, Effect of rice husk ash on the carbonation depth of concrete under different curing ages and humidity levels, J. Mater. Civ. Eng. 33 (2021), 04020427, https://doi.org/10.1061/(asce)mt.1943-5533.0003520.

[55] J.M. Marangu, C. Muturia M'thiruaine, M. Bediako, Physicochemical properties of hydrated portland cement blended with rice husk ash, J. Chem. 2020 (2020), https://doi.org/10.1155/2020/5304745.

[56] N. Nisar, J.A. Bhat, Experimental investigation of Rice Husk Ash on compressive strength, carbonation and corrosion resistance of reinforced concrete, Aust. J. Civ. Eng. (2020), https://doi.org/10.1080/14488353.2020.1838419.

[57] S.K. Antiohos, J.G. Tapali, M. Zervaki, J. Sousa-Coutinho, S. Tsimas, V. G. Papadakis, Low embodied energy cement containing untreated RHA, Constr. Build. Mater. 49 (2013) 455–463.

[58] S. Rukzon, P. Chindaprasirt, Strength and carbonation model of rice husk ash cement mortar with different fineness, J. Mater. Civ. Eng. 22 (2010) 253–259, https://doi.org/10.1061/(asce)0899-1561 (2010)22:3(253).

[59] P.G. Quedou, E. Wirquin, C. Bokhoree, Sustainable concrete: potency of sugarcane bagasse ash as a cementitious material in the construction industry, Case Stud. Constr. Mater. 14 (2021), https://doi.org/10.1016/j.cscm.2021.e00545.

[60] M.Z. Al-Mulali, H. Awang, H.P.S. Abdul Khalil, Z.S. Aljoumaily, The incorporation of oil palm ash in concrete as a means of recycling: a review, Cem. Concr. Compos. 55 (2015) 129–138, https://doi.org/10.1016/j.cemconcomp.2014.09.007.

[61] T. Matschei, B. Lothenbach, F.P. Glasser, The AFm phase in Portland cement, Cem. Concr. Res. 37 (2007) 118–130, https://doi.org/10.1016/j.cemconres.2006.10.010.

[62] L. Caneda-Martínez, W. Kunther, C. Medina, M.I. Sánchez de Rojas, M. Frías, Exploring sulphate resistance of coal mining waste blended cements through experiments and thermodynamic modelling, Cem. Concr. Compos. 121 (2021), https://doi.org/10.1016/j.cemconcomp.2021.104086.

[63] Z. Shi, B. Lothenbach, M.R. Geiker, J. Kaufmann, A. Leemann, S. Ferreiro, J. Skibsted, Experimental studies and thermodynamic modeling of the carbonation of portland cement, metakaolin and limestone mortars, Cem. Concr. Res. 88 (2016) 60–72, https://doi.org/10.1016/j.cemconres.2016.06.006.

[64] I.F. Sáez del Bosque, P. Van den Heede, N. De Belie, M.I. Sánchez de Rojas, C. Medina, Carbonation of concrete with construction and demolition waste based recycled aggregates and cement with recycled content, Constr. Build. Mater. 234 (2020), https://doi.org/10.1016/j.conbuildmat.2019.117336.

[65] S. Goto, K. Suenaga, T. Kado, M. Fukuhara, Calcium silicate carbonation products, J. Am. Ceram. Soc. 78 (1995) 2867–2872, https://doi.org/10.1111/j.1151-2916.1995.tb09057.x.

[66] M. Thiery, G. Villain, P. Dangla, G. Platret, Investigation of the carbonation front shape on cementitious materials: effects of the chemical kinetics, Cem. Concr. Res. 37 (2007) 1047–1058, https://doi.org/10.1016/j.cemconres.2007.04.002.

[67] M. Frías, S. Goñi, Accelerated carbonation effect on behaviour of ternary Portland cements, Compos. Part B Eng. 48 (2013) 122–128, https://doi.org/10.1016/J.COMPOSITESB.2012.12.008.

[68] B. Šavija, M. Luković, Carbonation of cement paste: understanding, challenges, and opportunities, Constr. Build. Mater. 117 (2016) 285–301, https://doi.org/10.1016/j.conbuildmat.2016.04.138.

[69] B. Wu, G. Ye, Development of porosity of cement paste blended with supplementary cementitious materials after carbonation, Constr. Build. Mater. 145 (2017) 52–61, https://doi.org/10.1016/j.conbuildmat.2017.03.176.

[70] L. De Ceukelaire, D. Van Nieuwenburg, Accelerated carbonation of a blast-furnace cement concrete, Cem. Concr. Res. 23 (1993) 442–452, https://doi.org/10.1016/0008-8846(93)90109-M.

[71] X. Fang, D. Xuan, P. Shen, C.S. Poon, Fast enhancement of recycled fine aggregates properties by wet carbonation, J. Clean. Prod. 313 (2021), https://doi.org/10.1016/j.jclepro.2021.127867.

[72] S. von Greve-Dierfeld, B. Lothenbach, A. Vollpracht, B. Wu, B. Huet, C. Andrade, C. Medina, C. Thiel, E. Gruyaert, H. Vanoutrive, I.F. Saéz del Bosque, I. Ignjatovic, J. Elsen, J.L. Provis, K. Scrivener, K.C. Thienel, K. Sideris, M. Zajac, N. Alderete, Ö. Cizer, P. Van den Heede, R.D. Hooton, S. Kamali-Bernard, S.A. Bernal, Z. Zhao, Z. Shi, N. De Belie, Understanding the carbonation of concrete with supplementary cementitious materials: a critical review by RILEM TC 281-CCC, Mater. Struct. Constr. 53 (2020), https://doi.org/10.1617/s11527-020-01558-w.

[73] T. Nishikawa, K. Suzuki, S. Ito, K. Sato, T. Takebe, Decomposition of synthesized ettringite by carbonation, Cem. Concr. Res. 22 (1992) 6–14, https://doi.org/10.1016/0008-8846(92)90130-N.

[74] C. Xiantuo, Z. Ruizhen, C. Xiaorong, Kinetic study of ettringite carbonation reaction, Cem. Concr. Res. 24 (1994) 1383–1389, https://doi.org/10.1016/0008-8846(94)90123-6.

[75] Q. Zhou, F.P. Glasser, Kinetics and mechanism of the carbonation of ettringite, Adv. Cem. Res. 12 (2000) 131–136, https://doi.org/10.1680/adcr.2000.12.3.131.

[76] A.E. Morandeau, C.E. White, In situ X-ray pair distribution function analysis of accelerated carbonation of a synthetic calcium-silicate-hydrate gel, J. Mater. Chem. A. 3 (2015) 8597–8605, https://doi.org/10.1039/c5ta00348b.

[77] A. Morandeau, M. Thiéry, P. Dangla, Investigation of the carbonation mechanism of CH and C-S-H in terms of kinetics, microstructure changes and moisture properties, Cem, Concr. Res. 56 (2014) 153–170, https://doi.org/10.1016/j.cemconres.2013.11.015.

[78] J. Xiao, J. Li, B. Zhu, Z. Fan, Experimental study on strength and ductility of carbonated concrete elements, Constr. Build. Mater. 16 (2002) 187–192, https://doi.org/10.1016/S0950-0618(01)00034-4.

[79] K. Ganesan, K. Rajagopal, K. Thangavel, Rice husk ash blended cement: assessment of optimal level of replacement for strength and permeability properties of concrete, Constr. Build. Mater. 22 (2008) 1675–1683, https://doi.org/10.1016/j.conbuildmat.2007.06.011.

[80] V. Jittin, S.N. Minnu, A. Bahurudeen, Potential of sugarcane bagasse ash as supplementary cementitious material and comparison with currently used rice husk ash, Constr. Build. Mater. 273 (2021), https://doi.org/10.1016/j.conbuildmat.2020.121679.

[81] J. Sousa Coutinho, The combined benefits of CPF and RHA in improving the durability of concrete structures, Cem. Concr. Compos. 25 (2003) 51–59, https://doi.org/10.1016/S0958-9465(01)00055-5.

[82] H. Kizhakkumodom Venkatanarayanan, P.R. Rangaraju, Effect of grinding of low-carbon rice husk ash on the microstructure and performance properties of blended cement concrete, Cem. Concr. Compos. 55 (2015) 348–363, https://doi.org/10.1016/j.cemconcomp.2014.09.021.

[83] V. Saraswathy, H.W. Song, Corrosion performance of rice husk ash blended concrete, Constr. Build. Mater. 21 (2007) 1779–1784, https://doi.org/10.1016/j.conbuildmat.2006.05.037.

[84] M. Zahedi, A.A. Ramezanianpour, A.M. Ramezanianpour, Evaluation of the mechanical properties and durability of cement mortars containing nanosilica and rice husk ash under chloride ion penetration, Constr. Build. Mater. 78 (2015) 354–361, https://doi.org/10.1016/j.conbuildmat.2015.01.045.

[85] B.S. Thomas, Green concrete partially comprised of rice husk ash as a supplementary cementitious material – a comprehensive review, Renew. Sustain. Energy Rev. 82 (2018) 3913–3923, https://doi.org/10.1016/j.rser.2017.10.081.

[86] S.A. Miller, P.R. Cunningham, J.T. Harvey, Rice-based ash in concrete: a review of past work and potential environmental sustainability, Resour. Conserv. Recycl. 146 (2019) 416–430, https://doi.org/10.1016/j.resconrec.2019.03.041.

[87] K. Ganesan, K. Rajagopal, K. Thangavel, Evaluation of bagasse ash as supplementary cementitious material, Cem. Concr. Compos. 29 (2007) 515–524, https://doi.org/10.1016/j.cemconcomp.2007.03.001.

[88] S. Rukzon, P. Chindaprasirt, Utilization of bagasse ash in high-strength concrete, Mater. Des. 34 (2012) 45–50, https://doi.org/10.1016/j.matdes.2011.07.045.

[89] B. Alsubari, P. Shafigh, M.Z. Jumaat, U.J. Alengaram, Palm oil fuel ash as a partial cement replacement for producing durable self-consolidating high-strength concrete, Arab. J. Sci. Eng. 39 (2014) 8507–8516, https://doi.org/10.1007/s13369-014-1381-3.

[90] P. Chindaprasirt, S. Rukzon, V. Sirivivatnanon, Resistance to chloride penetration of blended Portland cement mortar containing palm oil fuel ash, rice husk ash and fly ash, Constr. Build. Mater. 22 (2008) 932–938, https://doi.org/10.1016/j.conbuildmat.2006.12.001.

[91] P. Chindaprasirt, C. Chotetanorm, S. Rukzon, Use of palm oil fuel ash to improve chloride and corrosion resistance of high-strength and high-workability concrete, J. Mater. Civ. Eng. 23 (2011) 499–503, https://doi.org/10.1061/(asce)mt.1943-5533.0000187.

[92] P. Asha, A. Salman, R.A. Kumar, Experimental study on concrete with bamboo leaf ash, Int. J. Eng. Adv. Technol. (2014) 2249–8958.

[93] M.M. Hossain, M.R. Karim, M. Hasan, M.K. Hossain, M.F.M. Zain, Durability of mortar and concrete made up of pozzolans as a partial replacement of cement: a review, Constr. Build. Mater. 116 (2016) 128–140, https://doi.org/10.1016/j.conbuildmat.2016.04.147.

[94] A. Dousti, J.J. Beaudoin, M. Shekarchi, Chloride binding in hydrated MK, SF and natural zeolite-lime mixtures, Constr. Build. Mater. 154 (2017) 1035–1047, https://doi.org/10.1016/j.conbuildmat.2017.08.034.

[95] X. Shi, N. Xie, K. Fortune, J. Gong, Durability of steel reinforced concrete in chloride environments: an overview, Constr. Build. Mater. 30 (2012) 125–138, https://doi.org/10.1016/j.conbuildmat.2011.12.038.

[96] M.D.A.D.A. Thomas, R.D.D. Hooton, A. Scott, H. Zibara, The effect of supplementary cementitious materials on chloride binding in hardened cement paste, Cem. Concr. Res. 42 (2012) 1–7, https://doi.org/10.1016/j.cemconres.2011.01.001.

[97] C. Shi, X. Hu, X. Wang, Z. Wu, G. de Schutter, Effects of chloride ion binding on microstructure of cement pastes, J. Mater. Civ. Eng. 29 (2017), 04016183, https://doi.org/10.1061/(asce)mt.1943-5533.0001707.

[98] U. Birnin-Yauri, F. Glasser, Friedel's salt, $Ca_2Al(OH)_6(Cl,OH)\cdot 2H_2O$: its solid solutions and their role in chloride binding, Cem. Concr. Res. 28 (1998) 1713–1723, https://doi.org/10.1016/S0008-8846(98)00162-8.

[99] L. Caneda-Martínez, M. Frías, C. Medina, M.I. Sanchez, N. Rebolledo, J. Sánchez, Evaluation of chloride transport in blended cement mortars containing coal mining waste, Constr. Build. Mater. 190 (2018) 200–210, https://doi.org/10.1016/j.conbuildmat.2018.09.158.

[100] Z. Shi, M.R. Geiker, B. Lothenbach, K. De Weerdt, S.F. Garzón, K. Enemark-Rasmussen, J. Skibsted, Friedel's salt profiles from thermogravimetric analysis and thermodynamic modelling of Portland cement-based mortars exposed to sodium chloride solution, Cem. Concr. Compos. 78 (2017) 73–83, https://doi.org/10.1016/j.cemconcomp.2017.01.002.

[101] M.D.A. Thomas, R.D. Hooton, A. Scott, H. Zibara, The effect of supplementary cementitious materials on chloride binding in hardened cement paste, Cem. Concr. Res. 42 (2012) 1–7, https://doi.org/10.1016/j.cemconres.2011.01.001.

[102] L.-O. Nilson, E. Poulsen, P. Sandberg, H.E. Sorensen, O. Klinghoffer, Chloride Penetration into Concrete State-Of-The-Art: Transport Processes, Corrosion Initiation, Test Methods and Prediction Models, 1996, https://doi.org/10.13140/RG.2.1.2771.7526.

[103] Z. Zhu, H. Chu, M. zhi Guo, M. Shen, L. Jiang, L. Yu, Effect of silica fume and fly ash on the stability of bound chlorides in cement mortar during electrochemical chloride extraction, Constr. Build. Mater. 256 (2020), https://doi.org/10.1016/j.conbuildmat.2020.119481.

[104] J.J. Beaudoin, V.S. Ramachandran, R.F. Feldman, Interaction of chloride and CSH, Cem. Concr. Res. 20 (1990) 875–883, https://doi.org/10.1016/0008-8846(90)90049-4.

[105] H. Zibara, R.D. Hooton, M.D.A. Thomas, K. Stanish, Influence of the C/S and C/A ratios of hydration products on the chloride ion binding capacity of lime-SF and lime-MK mixtures, Cem. Concr. Res. 38 (2008) 422–426, https://doi.org/10.1016/j.cemconres.2007.08.024.

[106] A. Dousti, J.J. Beaudoin, M. Shekarchi, Chloride binding in hydrated MK, SF and natural zeolite-lime mixtures, Constr. Build. Mater. 154 (2017) 1035–1047, https://doi.org/10.1016/j.conbuildmat.2017.08.034.

[107] F. Massazza, Pozzolanic cements, Cem. Concr. Compos. 15 (1993) 185–214, https://doi.org/10.1016/0958-9465(93)90023-3.

[108] R. Loser, B. Lothenbach, A. Leemann, M. Tuchschmid, Chloride resistance of concrete and its binding capacity – comparison between experimental results and thermodynamic modeling, Cem. Concr. Compos. 32 (2010) 34–42, https://doi.org/10.1016/j.cemconcomp.2009.08.001.

[109] P. Azarsa, R. Gupta, Electrical resistivity of concrete for durability evaluation: a review, Adv. Mater. Sci. Eng. 2017 (2017), https://doi.org/10.1155/2017/8453095.

[110] C. Andrade, M. Castellote, R. D'Andrea, Chloride aging factor of concrete measured by means of resistivity, in: V. Peixoto de Freitas, H. Corvacho, M. Lacasse (Eds.), Proc. XII DBMC Int. Conf. Durab. Build. Mater. Components, FEUP Ediçoes, Porto, 2011, pp. 1–8.

[111] C. Andrade, M. Castellote, R. D'Andrea, The use of resistivity for measuring aging of chloride diffusion coefficient, in: M.G. Alexander, A. Bertron (Eds.), Proc. Pro063 RILEM TC 211-PAE Final Conf. Concr. Aggress. Aqueous Environ. - Performance, Test. Model, RILEM Publications SARL, Toulouse, 2009, pp. 564–571.

[112] R.M. Faysal, M. Maslehuddin, M. Shameem, S. Ahmad, S.K. Adekunle, Effect of mineral additives and two-stage mixing on the performance of recycled aggregate concrete, J. Mater. Cycles Waste Manag. 22 (2020) 1587–1601, https://doi.org/10.1007/s10163-020-01048-9.

[113] A. Muthadhi, S. Kothandaraman, Experimental investigations of performance characteristics of rice husk ash–blended concrete, J. Mater. Civ. Eng. 25 (2013) 1115–1118, https://doi.org/10.1061/(asce)mt.1943-5533.0000656.

[114] A.L.G. Gastaldini, M.P. Da Silva, F.B. Zamberlan, C.Z. Mostardeiro Neto, Total shrinkage, chloride penetration, and compressive strength of concretes that contain clear-colored rice husk ash, Constr. Build. Mater. 54 (2014) 369–377, https://doi.org/10.1016/j.conbuildmat.2013.12.044.

[115] W. Müllauer, R.E. Beddoe, D. Heinz, Sulfate attack expansion mechanisms, Cem. Concr. Res. 52 (2013) 208–215, https://doi.org/10.1016/j.cemconres.2013.07.005.

[116] L. Caneda-Martínez, M. Frías, J. Sanchez de Rojas, Ma Sánchez, C. Medina, SP-349_21: industrial mineral waste as an alternative pozzolan for the design of eco-efficient binary cements: impact on physical properties and chloride resistance, in: A. Tagnit-Hamou (Ed.), 11th ACI/RILEM Int. Conf. Cem. Mater. Altern, . Bind. Sustain. Concr., 2021, pp. 301–320.

[117] S. Goñi, M. Frias, R. Vigil de la Villa, R. García, Sodium chloride effect on durability of ternary blended cement. Microstructural characterization and

strength, Compos. Part B Eng. 54 (2013) 163–168, https://doi.org/10.1016/j.compositesb.2013.05.002.
[118] U.M. Angst, B. Elsener, Chloride threshold values in concrete - a look back and ahead, in: Am. Concr. Institute, ACI Spec. Publ., 2016, pp. 1–12.
[119] M.D.A. Thomas, J.D. Matthews, Performance of pfa concrete in a marine environment - 10-year results, Cem. Concr. Compos. 26 (2004) 5–20, https://doi.org/10.1016/S0958-9465(02)00117-8.
[120] L. Caneda-Martínez, J. Sánchez, C. Medina, M. Isabel Sánchez de Rojas, J. Torres, M. Frías, Reuse of coal mining waste to lengthen the service life of cementitious matrices, Cem. Concr. Compos. 99 (2019) 72–79, https://doi.org/10.1016/j.cemconcomp.2019.03.007.